



APOGEE-2S Discovery of Light- and Heavy-element Abundance Correlations in the Bulge Globular Cluster NGC 6380

José G. Fernández-Trincado¹, Timothy C. Beers², Beatriz Barbuy³, Szabolcs Mészáros^{4,5,6}, Dante Minniti^{7,8}, Verne V. Smith⁹, Katia Cunha^{10,11}, Sandro Villanova¹², Doug Geisler^{12,13,14}, Steven R. Majewski¹⁵, Leticia Carigi¹⁶, Baitian Tang¹⁷, Christian Moni Bidin¹, and Katherine Vieira¹⁸

¹ Instituto de Astronomía, Universidad Católica del Norte, Avenida Angamos 0610, Antofagasta, Chile; jfernandezt87@gmail.com

² Department of Physics and JINA Center for the Evolution of the Elements, University of Notre Dame, Notre Dame, IN 46556, USA

³ Universidade de São Paulo, IAG, Rua do Matão 1226, Cidade Universitária, São Paulo 05508-900, Brazil

⁴ ELTE Eötvös Loránd University, Gothard Astrophysical Observatory, 9700 Szombathely, Szent Imre H. st. 112, Hungary

⁵ MTA-ELTE Lendület Milky Way Research Group, Hungary

⁶ MTA-ELTE Exoplanet Research Group, Hungary

⁷ Departamento de Cs. Físicas, Facultad de Ciencias Exactas, Universidad Andrés Bello, Avenida Fernández Concha 700, Las Condes, Santiago, Chile

⁸ Vatican Observatory, V00120 Vatican City State, Italy

⁹ NSF's NOIRLab, 950 N. Cherry Avenue, Tucson, AZ 85719, USA

¹⁰ Steward Observatory, Department of Astronomy, University of Arizona, Tucson, AZ 85721, USA

¹¹ Observatório Nacional, MCTI, Rio de Janeiro, Brazil

¹² Departamento de Astronomía, Casilla 160-C, Universidad de Concepción, Concepción, Chile

¹³ Department of Astronomy—Universidad de La Serena—Avenida Juan Cisternas, 1200 North, La Serena, Chile

¹⁴ Instituto de Investigación Multidisciplinario en Ciencia y Tecnología, Universidad de La Serena. Benavente 980, La Serena, Chile

¹⁵ Department of Astronomy, University of Virginia, Charlottesville, VA 22904, USA

¹⁶ Instituto de Astronomía, Universidad Nacional Autónoma de México, A.P. 70-264, 04510, Ciudad de México, México

¹⁷ School of Physics and Astronomy, Sun Yat-sen University, Zhuhai 519082, People's Republic of China

¹⁸ Instituto de Astronomía y Ciencias Planetarias, Universidad de Atacama, Copayapu 485, Copiapó, Chile

Received 2021 July 6; revised 2021 August 7; accepted 2021 August 9; published 2021 August 26

Abstract

We derive abundance ratios for nine stars in the relatively high-metallicity bulge globular cluster NGC 6380. We find a mean cluster metallicity between $[\text{Fe}/\text{H}] = -0.80$ and -0.73 , with no clear evidence for a variation in iron abundances beyond the observational errors. Stars with strongly enhanced $[\text{N}/\text{Fe}]$ abundance ratios populate the cluster and are anticorrelated with $[\text{C}/\text{Fe}]$, trends that are considered a signal of the multiple-population phenomenon in this cluster. We detect an apparent intrinsic star-to-star spread ($\gtrsim 0.27$ dex) in the slow neutron-capture process element (*s*-element) Ce II. Moreover, the $[\text{Ce}/\text{Fe}]$ abundance ratio exhibits a likely correlation with $[\text{N}/\text{Fe}]$, and a somewhat weaker correlation with $[\text{Al}/\text{Fe}]$. If confirmed, NGC 6380 could be the first high-metallicity globular cluster where a N–Ce correlation is detected. Furthermore, this correlation suggests that Ce may also be an element involved in the multiple-population phenomenon. Currently, a consensus interpretation for the origin of the this apparent N–Ce correlation in high-metallicity clusters is lacking. We tentatively suggest that it could be reproduced by different channels—low-mass asymptotic giant branch stars in the high-metallicity regime or fast-rotating massive stars (“spinstars”), due to the rotational mixing. It may also be the cumulative effect of several pollution events including the occurrence of peculiar stars. Our findings should guide stellar nucleosynthesis models, in order to understand the reasons for its apparent exclusivity in relatively high-metallicity globular clusters.

Unified Astronomy Thesaurus concepts: Globular star clusters (656); Stellar abundances (1577)

1. Introduction

For over a decade, spectroscopic and photometric data have revealed that virtually all studied Milky Way (MW) globular clusters (GCs) host (at least) two main groups of stars with a complex chemical-enrichment history—the so-called multiple-population (MP) phenomenon in GCs, which are commonly distinguished by their different light-element enrichment (see the review by Bastian & Lardo 2018).

In general, GC stars have been shown to exhibit C, N, O, Mg, Na, and Al variations (see, e.g., Carretta et al. 2009; Mészáros et al. 2015, 2020; Pancino et al. 2017; Schiavon et al. 2017; Masseron et al. 2019; Nataf et al. 2019; Geisler et al. 2021 and

references therein), with a few exceptions exhibiting K and Ca abundance variations (Cohen & Kirby 2012; Carretta et al. 2013; Carretta & Bragaglia 2021), as well as internal variations in the heavy elements produced via slow neutron-capture reactions (Masseron et al. 2019; Mészáros et al. 2020; Marino et al. 2021). In addition, the most common feature identified so far in almost all the GCs are the clear anticorrelations Na–O and N–C, Mg–K, and Al–Mg (see Mucciarelli et al. 2015; Pancino et al. 2017; Masseron et al. 2019; Mészáros et al. 2020), some of them depending on the GC mass and metallicity (see, e.g., Pancino et al. 2017; Carretta & Bragaglia 2021), as well as correlations between N–Al, Al–Si, and others (see, e.g., Masseron et al. 2019; Mészáros et al. 2020).

Even though a broad range of polluters (see Renzini et al. 2015 for a review) have been proposed to explain these apparent abundance variations in GCs, a clear consensus on the origin of the nucleosynthetic pathways that were responsible for the



Original content from this work may be used under the terms of the [Creative Commons Attribution 4.0 licence](https://creativecommons.org/licenses/by/4.0/). Any further distribution of this work must maintain attribution to the author(s) and the title of the work, journal citation and DOI.

puzzling (anti) correlations among light elements is still under debate.

In this Letter, we analyze recent APOGEE-2S data of the heavily reddened ($E(B - V) = 1.07$; Ortolani et al. 1998) bulge GC NGC 6380 (Djorgovski & Meylan 1993), also known as Tonantzintla 1 and Pismis 25—(Pišmiš 1959).

We suggest that a correlation between Al and N with Ce could be present in NGC 6380, as suggested by the Pearson and Spearman correlation coefficients, indicating that the multiple-population phenomenon includes this *s*-process element as well as the other traditional light elements associated with it. However, additional observations are needed to confirm this finding and to gain more confidence in this assertion. This finding could play an important role as a new entry among the chemical anomalies in GCs at metallicity around $[\text{Fe}/\text{H}] = -0.73$, and will supply useful additional constraints to theoretical models to infer more appropriate scenarios for the origin of MPs in GCs.

2. Data

We use data from the sixteenth data release (DR16; Ahumada et al. 2020) of the second generation of the Apache Point Observatory Galactic Evolution Experiment (APOGEE-2) survey (Majewski et al. 2017), which is one of the programs in the Sloan Digital Sky Survey (SDSS-IV; Blanton et al. 2017).

The APOGEE-2 instruments are high-resolution ($R \sim 22,000$), near-infrared (collecting most of the *H*band: 15145–16960 Å; vacuum wavelengths) spectrographs (Wilson et al. 2019) that operate on the Sloan 2.5 m telescope (Gunn et al. 2006) at the Apache Point Observatory (APOGEE-2N) and on the Irénée du Pont 2.5 m telescope (Bowen & Vaughan 1973) at Las Campanas Observatory (APOGEE-2S). The targeting strategy of the APOGEE-2 survey is summarized in Zasowski et al. (2017), while spectra are reduced as described in Nidever et al. (2015), and analyzed using the APOGEE Stellar Parameters and Chemical Abundance Pipeline (ASPCAP; García Pérez et al. 2016). The libraries of synthetic spectra and the *H*-band line list used are described in Zamora et al. (2015) and Smith et al. (2021), respectively.

2.1. NGC 6380

The APOGEE-2S plug-plate containing the NGC 6380 stars was centered on $(l, b) \sim (350^\circ, -04^\circ)$ as part of the bulge program survey, and 13 of 506 science fibers were located in the innermost region ($\lesssim 2 \times r_{h,m}$) of NGC 6380, as shown in Figure 1(a).

Figures 1(b)–(d) reveal that our stars share the same kinematic and astrometric properties as NGC 6380 (also listed in Table 1), and are positioned along the red giant branch (RGB) of the cluster. The nominal proper motions of the cluster, highlighted in Figure 1(b), have been taken from Vasiliev & Baumgardt (2021)— $(\mu_\alpha \cos(\delta), \mu_\delta) = (-2.183 \pm 0.031 \text{ mas yr}^{-1}, -3.233 \pm 0.03 \text{ mas yr}^{-1})$, while the structural parameters of the cluster are taken from Cohen et al. (2021)— $(r_{h,m}, r_t) = (83'', 751'')$.

It is important to note that 12 of the 13 observed cluster stars in our sample have spectra with a high signal-to-noise ratio (S/N), $>75 \text{ pixel}^{-1}$, except for one star, 2M17342736–3905102, which has a spectrum with an S/N = 29 pixel^{-1} and is the faintest star in Figure 1(d).

In the following, we use all stars to provide reliable and precise ($<1 \text{ km s}^{-1}$) radial velocities for cluster-member confirmation, but

limit ourselves to the 12 higher S/N stars for the abundance analysis, as highlighted in Figure 1(c). It is also important to note that other sources that fall inside the box highlighted in Figure 1(c) are foreground/background stars with other properties that are not compatible with NGC 6380 stars.

3. Elemental Abundances

Atmospheric parameters were adopted from the DR16 (uncalibrated) T_{eff} and $\log g$ determined by the ASPCAP pipeline through the best fits between the synthetic and observed spectra for the entire APOGEE region; and also by applying a simple approach of fixing T_{eff} and $\log g$ to values determined independently of spectroscopy. We obtain T_{eff} and $\log g$ from photometry in the same manner as described in Romero-Colmenares et al. (2021), i.e., we first derived the differentially reddening-corrected color–magnitude diagram (CMD) of Figure 1(d). We then horizontally projected the position of each observed star until it intersected the PARSEC (Bressan et al. 2012) isochrone (chosen to be 12 Gyr), and assumed T_{eff} and $\log g$ to be the temperature and gravity of the point of the isochrones that have the same *G* magnitude as the star. We underline the fact that, for highly reddened objects like NGC 6380, the absorption correction depends on the spectral energy distribution of the star, i.e., on its temperature. For this reason, we applied a temperature-dependent absorption correction to the isochrone. Without this, it is not possible to obtain a proper fit of the RGB, especially of the upper and cooler part. The adopted atmospheric parameters are listed in Table 1. It is important to note that the target stars are not compatible with both sets of parameters. This issue does not strongly affect the mean derived $[\text{X}/\text{Fe}]$ abundance ratios in NGC 6380, but some chemical species, such as oxygen, magnesium, and cerium, are more sensitive to these discrepancies, as can be appreciated in Table 1. We highlight that our determined abundance ratios by adopting atmospheric parameters from photometry are likely more reliable and realistic, as the set of photometry parameters better reflect the real distribution of the stars on the CMD.

With the fixed T_{eff} and $\log g$, the first step consisted of determining the metallicity from selected Fe I lines, the microturbulence velocity (ξ), and the convolution parameter with the Brussels Automatic Stellar Parameter (BACCHUS) code (Masseron et al. 2016). Thus, the metallicity provided is the average abundance of selected Fe I lines, while the microturbulence velocity is obtained by minimizing the trend of Fe abundances against their reduced equivalent width, and the convolution parameter represents the total effect of the instrument resolution.

Chemical abundances were derived from a local thermodynamic equilibrium analysis using the BACCHUS code and the MARCS model atmospheres (Gustafsson et al. 2008) for likely NGC 6380 stars, following the same methodology as described in Fernández-Trincado et al. (2019, 2020, 2021a, 2021b, 2021c). This approach allows us to minimize the number of caveats present in the determinations of ASPCAP abundance ratios toward GCs (see, e.g., Masseron et al. 2019; Mészáros et al. 2020). For APOGEE-2 spectra, we infer chemical abundances for the Fe-peak (Fe, Ni), odd-Z (Al, K), α - (O, Mg, Si, Ca, Ti), light- (C, N), and *s*-process (Ce) elements.

Figure 2 shows two examples of the excellent quality of the APOGEE-2 spectra and the success of the fitting procedure for selected atomic and molecular lines for two arbitrarily selected members of NGC 6380. The same figure also indicates the

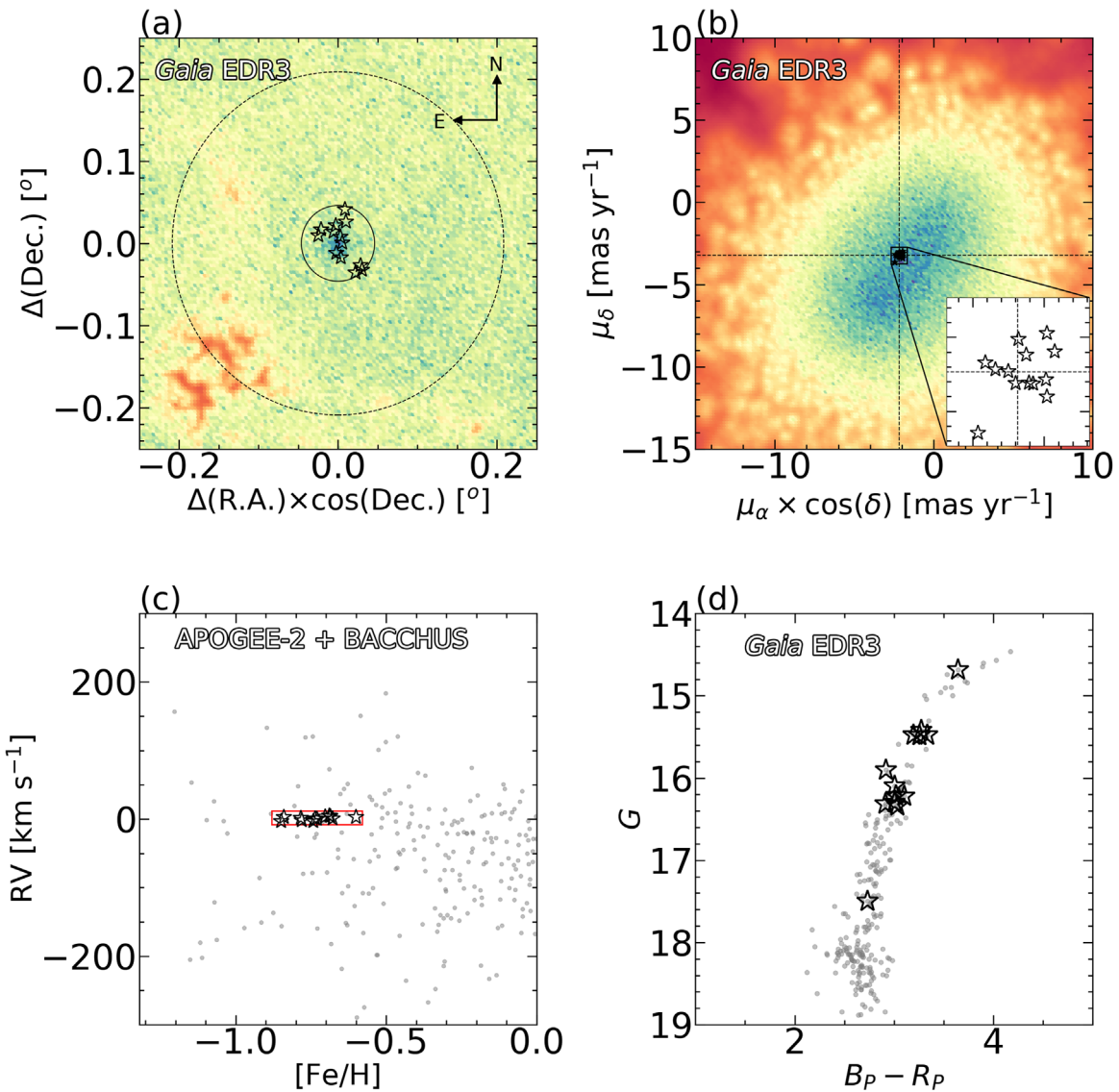


Figure 1. Main properties of NGC 6380 stars. Panel (a): sky position of stars centered on NGC 6380. Stars analyzed in this work are marked with star symbols, while the overlaid large and small circles refer to the cluster tidal radius (r_t) and twice the half-mass radius ($2 \times r_{h,m}$), respectively. Density maps in panel (a) highlight the stars in the Gaia EDR3 footprint within a box of 0.5×0.5 deg centered on NGC 6380, while panel (b) shows the distribution in PMs for stars toward the field of NGC 6380, with the inner window highlighting the distribution of our sample within a 0.5 mas yr^{-1} radius around the nominal PMs of the cluster highlighted with black dashed lines. Panel (c): radial velocity vs. $[\text{Fe}/\text{H}]$ of our member stars compared to APOGEE-2 field stars. The metallicity of our targets have been determined with BACCHUS, while those for field stars are from the ASPCAP pipeline. The red box limited by ± 0.15 dex and $\pm 10 \text{ km s}^{-1}$, centered on $[\text{Fe}/\text{H}] = -0.73$ and $\text{RV} = +1.92 \text{ km s}^{-1}$, encloses our potential cluster members. Panel (d): differential-reddening-corrected color-magnitude diagram in the Gaia bands for cluster stars with a membership probability larger than 90% (see, e.g., Vasiliev & Baumgardt 2021).

detectable $^{12}\text{C}^{16}\text{O}$, ^{16}OH , $^{12}\text{C}^{14}\text{N}$, and Ce II lines (cyan bands in Figure 2).

The resulting elemental-abundance ratios are listed in Table 1, which are scaled to the solar reference values from Asplund et al. (2005).

4. Results and Discussion

NGC 6380 has been examined previously in Horta et al. (2020) using ASPCAP/APOGEE DR16 results. In that study they investigated if GCs formed in situ or from external origin. Based on the calibrated ASPCAP $[\text{Si}/\text{Fe}]$ abundance ratios, they concluded that NGC 6380 formed in situ and did not have an extragalactic origin. However, it is important to note that their ASPCAP determinations of $[\text{Si}/\text{Fe}]$ for NGC 6380 are ~ 0.15 dex lower, on average, than our determinations. This

discrepancy could be due to some issues with the accuracy (zero-point) of ASPCAP abundances toward GCs, limits of the model grid, and/or the difficulty of fitting lines where the intensity is comparable to the variance. Furthermore, the ASPCAP pipeline uses a global fit to the continuum in the three detector chips independently, while the BACCHUS pipeline places the pseudo-continuum in a region around the lines of interest. Thus, we believe that our manual method is likely more reliable, since it avoids possible shifts in the continuum location due to imperfections in the spectral subtraction along the full spectral range (see, e.g., Masseron et al. 2019 for details).

Figure 3 summarizes the chemical makeup for likely members of NGC 6380 in a violin representation, which is compared to the elemental abundances of 47 Tucanae stars

Table 1
Main Kinematics, Astrometric Properties, and Elemental Abundances for Likely NGC 6380 Members

APOGEE–Id	G	B_P	R_P	S/N	RV (km s ⁻¹)	$\mu_\alpha \cos(\delta)$ (mas yr ⁻¹)	μ_δ (mas yr ⁻¹)	T_{eff} (K)	log g (cgs)	ξ_r (km s ⁻¹)	[C/Fe]	[N/Fe]	[O/Fe]	[Mg/ Fe]	[Al/ Fe]	[Si/ Fe]	[K/Fe]	[Ca/ Fe]	[Ti/ Fe]	[Fe/H]	[Ni/ Fe]	[Ce/ Fe]
				(pixel ⁻¹)	(km s ⁻¹)	(mas yr ⁻¹)	(mas yr ⁻¹)	(K)	(cgs)	(km s ⁻¹)												
Photometry																						
2M17342588 –3901406	14.69	16.99	13.35	234	+3.63	–2.25	–3.22	3584	0.26	2.37	–0.18	+0.49	+0.17	+0.18	+0.22	+0.30	+0.39	+0.13	+0.19	–0.78	+0.02	–0.06
2M17341922 –3906052	15.42	17.41	14.14	160	+3.73	–2.12	–3.11	3866	0.77	1.56	–0.18	+0.29	+0.39	+0.48	–0.02	+0.37	+0.18	+0.29	+0.20	–0.61	–0.10	+0.01
2M17342921 –3904514	15.49	17.38	14.12	158	+2.16	–1.98	–3.39	3850	0.74	2.50	–0.51	+1.13	–0.10	+0.20	+0.52	+0.33	+0.51	+0.23	+0.35	–0.79	+0.10	+0.08
2M17343616 –3903344	15.48	17.41	14.22	145	–1.28	–2.34	–3.21	3890	0.81	2.31	–0.53	+1.27	+0.14	+0.33	+0.29	+0.36	+0.27	+0.21	+0.31	–0.85	+0.07	+0.15
2M17343025 –3903190	15.48	17.49	14.16	144	+0.63	–2.10	–3.30	3859	0.75	2.48	–0.59	+0.99	–0.09	+0.31	+0.44	+0.33	+0.28	+0.28	+0.25	–0.85	+0.15	+0.16
2M17342693 –3904060	16.22	17.79	14.69	105	–2.79	–2.46	–3.64	4073	1.14	2.21	–0.07	+0.79	+0.21	+0.27	+0.19	+0.39	+0.13	+0.14	+0.16	–0.90	+0.13	+0.07
2M17342541 –3902338	15.90	17.60	14.69	88	–2.61	–2.07	–3.31	4059	1.12	2.27	–0.06	+0.63	–0.01	+0.33	+0.50	+0.42	+0.19	+0.30	+0.28	–0.86	+0.14	+0.07
2M17342767 –3903405	16.29	17.96	14.95	87	+4.21	–2.41	–3.16	4125	1.24	2.10	–0.53	+1.02	+0.01	+0.36	+0.52	+0.33	+0.18	+0.23	+0.25	–0.79	+0.12	+0.21
2M17341969 –3905457	16.09	17.87	14.86	85	+1.55	–2.19	–3.30	4099	1.19	2.14	–0.59	+1.23	–0.15	+0.32	+0.54	+0.36	+0.20	+0.27	+0.25	–0.83	+0.10	...
2M17342177 –3906173	16.34	18.13	15.09	84	+5.04	–2.18	–3.01	4166	1.31	2.10	–0.35	+0.92	...	+0.31	+0.50	+0.37	+0.11	+0.27	+0.26	–0.78	+0.07	...
2M17342943 –3902500	16.22	17.99	14.97	77	+1.26	–1.98	–3.28	4136	1.26	2.01	–0.60	+1.24	–0.12	+0.32	+0.73	+0.42	+0.05	+0.26	+0.26	–0.76	+0.02	+0.14
2M17343521 –3903091	16.31	17.99	15.08	75	+5.35	–1.98	–2.97	4174	1.33	2.11	–0.97	+1.90	–0.16	+0.22	+0.18	+0.43	+0.01	–0.01	+0.55	–0.87	–0.01	...
2M17342736 –3905102	17.50	18.88	16.15	29	+4.06	–1.92	–3.09
Mean											–0.43	+0.99	+0.03	+0.30	+0.38	+0.37	+0.21	+0.22	+0.28	–0.80	+0.07	+0.09
1 σ											0.22	0.33	0.16	0.06	0.17	0.04	0.11	0.07	0.06	0.04	0.06	0.07
Spectroscopy																						
2M17342588 –3901406	14.69	16.99	13.35	234	+3.63	–2.25	–3.22	3627	0.66	2.32	+0.07	+0.58	+0.32	+0.17	+0.24	+0.37	+0.21	+0.18	+0.27	–0.84	+0.05	+0.07
2M17341922 –3906052	15.42	17.41	14.14	160	+3.73	–2.12	–3.11	3783	0.97	1.51	–0.11	+0.15	+0.22	+0.32	+0.08	+0.38	+0.12	+0.18	+0.20	–0.60	–0.12	+0.01
2M17342921 –3904514	15.49	17.38	14.12	158	+2.16	–1.98	–3.39	4055	1.50	2.55	–0.26	+1.30	+0.25	+0.13	+0.53	+0.33	+0.37	+0.33	+0.53	–0.78	+0.16	+0.43
2M17343616 –3903344	15.48	17.41	14.22	145	–1.28	–2.34	–3.21	3983	1.44	2.34	–0.34	+1.22	+0.22	+0.12	+0.24	+0.38	+0.25	+0.18	+0.40	–0.78	+0.12	+0.34
2M17343025 –3903190	15.48	17.49	14.16	144	+0.63	–2.10	–3.30	4120	1.60	2.52	–0.51	+1.46	+0.18	+0.14	+0.41	+0.33	+0.29	+0.33	+0.54	–0.72	+0.15	+0.55
2M17342693 –3904060	16.22	17.79	14.69	105	–2.79	–2.46	–3.64	4146	1.61	2.25	+0.07	+0.73	+0.28	+0.13	+0.17	+0.39	+0.12	+0.12	+0.20	–0.85	+0.15	+0.23
2M17342541 –3902338	15.90	17.60	14.69	88	–2.61	–2.07	–3.31	4282	1.94	2.22	–0.23	+1.27	+0.20	+0.12	+0.44	+0.38	+0.20	+0.32	+0.43	–0.74	+0.15	+0.40
2M17342767 –3903405	16.29	17.96	14.95	87	+4.21	–2.41	–3.16	4311	2.05	2.06	–0.25	+1.22	+0.17	+0.14	+0.39	+0.31	+0.19	+0.23	+0.46	–0.70	+0.15	+0.46
2M17341969 –3905457	16.09	17.87	14.86	85	+1.55	–2.19	–3.30	4366	2.16	2.09	–0.01	+0.89	+0.20	+0.12	+0.67	+0.34	+0.26	+0.31	+0.48	–0.73	+0.17	...
2M17342177 –3906173	16.34	18.13	15.09	84	+5.04	–2.18	–3.01	4361	2.14	2.01	–0.09	+0.78	...	+0.09	+0.39	+0.37	+0.15	+0.28	+0.48	–0.68	+0.15	...
2M17342943 –3902500	16.22	17.99	14.97	77	+1.26	–1.98	–3.28	4363	2.07	1.90	–0.13	+1.05	+0.18	+0.08	+0.69	+0.37	+0.08	+0.29	+0.53	–0.67	+0.07	+0.39
2M17343521 –3903091	16.31	17.99	15.08	75	+5.35	–1.98	–2.97	4633	2.05	2.50	–0.69	+1.72	+0.45	+0.23	+0.35	+0.35	+0.09	+0.07	+0.26	–0.68	+0.02	...
	17.50	18.88	16.15	29	+4.06	–1.92	–3.09

Table 1
(Continued)

APOGEE–Id	G	B_P	R_P	S/N	RV (km s ⁻¹)	$\mu_\alpha \cos(\delta)$ (mas yr ⁻¹)	μ_δ (mas yr ⁻¹)	T_{eff} (K)	log g (cgs)	ξ_r (km s ⁻¹)	[C/Fe]	[N/Fe]	[O/Fe]	[Mg/ Fe]	[Al/ Fe]	[Si/ Fe]	[K/Fe]	[Ca/ Fe]	[Ti/ Fe]	[Fe/H]	[Ni/ Fe]	[Ce/ Fe]	
2M17342736 –3905102																							
Mean					+1.92						-0.21	+1.03	+0.25	+0.15	+0.39	+0.36	+0.20	+0.24	+0.40	-0.73	+0.11	+0.32	
1 σ					2.84						0.20	0.32	0.06	0.04	0.17	0.02	0.08	0.08	0.14	0.06	0.06	0.17	
Typical uncertainties																							
2M17342588 –3901406	14.69	16.99	13.35	234	+3.63	-2.25	-3.22	3627	0.66	2.32	0.29	0.15	0.22	0.13	0.12	0.16	0.16	0.13	0.12	0.19	0.18	0.12	
2M17341922 –3906052	15.42	17.41	14.14	160	+3.73	-2.12	-3.11	3783	0.97	1.51	0.19	0.21	0.22	0.16	0.20	0.05	0.07	0.12	0.23	0.14	0.12	0.13	
2M17342921 –3904514	15.49	17.38	14.12	158	+2.16	-1.98	-3.39	4055	1.50	2.55	0.15	0.17	0.18	0.10	0.12	0.12	0.12	0.11	0.16	0.15	0.18	0.07	
2M17343616 –3903344	15.48	17.41	14.22	145	-1.28	-2.34	-3.21	3983	1.44	2.34	0.14	0.21	0.18	0.09	0.13	0.11	0.07	0.09	0.18	0.12	0.08	0.10	
2M17343025 –3903190	15.48	17.49	14.16	144	+0.63	-2.10	-3.30	4120	1.60	2.52	0.14	0.16	0.19	0.08	0.14	0.11	0.06	0.09	0.14	0.13	0.14	0.11	
2M17342693 –3904060	16.22	17.79	14.69	105	-2.79	-2.46	-3.64	4146	1.61	2.25	0.14	0.18	0.12	0.10	0.14	0.10	0.06	0.06	0.19	0.11	0.09	0.06	
2M17342541 –3902338	15.90	17.60	14.69	88	-2.61	-2.07	-3.31	4282	1.94	2.22	0.15	0.26	0.19	0.12	0.11	0.15	0.07	0.12	0.18	0.11	0.13	0.08	
2M17342767 –3903405	16.29	17.96	14.95	87	+4.21	-2.41	-3.16	4311	2.05	2.06	0.07	0.15	0.16	0.11	0.07	0.08	0.21	0.07	0.13	0.10	0.10	0.10	
2M17341969 –3905457	16.09	17.87	14.86	85	+1.55	-2.19	-3.30	4366	2.16	2.09	0.21	0.26	0.17	0.11	0.19	0.11	0.06	0.10	0.17	0.13	0.10	...	
2M17342177 –3906173	16.34	18.13	15.09	84	+5.04	-2.18	-3.01	4361	2.14	2.01	0.04	0.19	...	0.11	0.10	0.12	0.06	0.09	0.15	0.11	0.09	...	
2M17342943 –3902500	16.22	17.99	14.97	77	+1.26	-1.98	-3.28	4363	2.07	1.90	0.24	0.27	0.19	0.10	0.12	0.10	0.11	0.11	0.19	0.14	0.10	0.12	
2M17343521 –3903091	16.31	17.99	15.08	75	+5.35	-1.98	-2.97	4633	2.05	2.50	0.20	0.15	0.26	0.08	0.06	0.13	0.07	0.03	0.13	0.12	0.11	...	
2M17342736 –3905102	17.50	18.88	16.15	29	+4.06	-1.92	-3.09	

Note. The first part of the table shows the resulting elemental abundance determined by adopting atmospheric parameters from photometry, while the second part shows that from the spectroscopy (see Section 3). The Typical uncertainties were computed in the same manner as described in Fernández-Trincado et al. (2019). 1σ is defined as (84th – 16th)/2. The bold values are the cluster mean values of each chemical species as indicated in the first column.

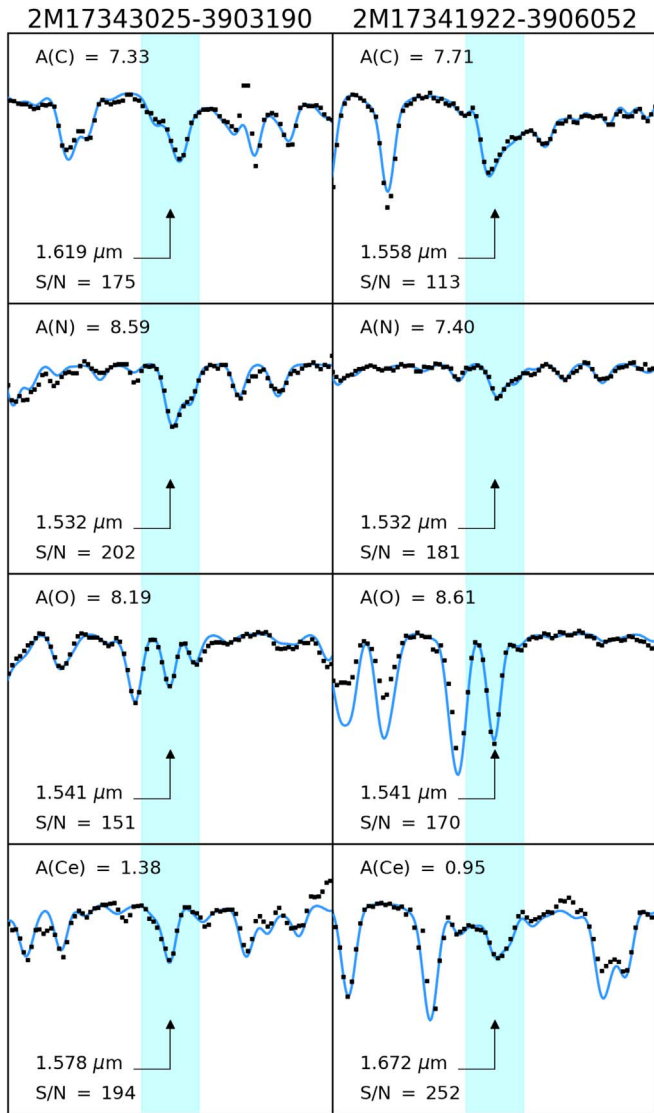


Figure 2. Example of the detection of $^{12}\text{C}^{16}\text{O}$, ^{16}OH , $^{12}\text{C}^{14}\text{N}$, and Ce II lines in two arbitrarily selected stars in our sample. A portion of the spectral synthesis is shown for the determination of the $[\text{C}/\text{Fe}]$, $[\text{N}/\text{Fe}]$, $[\text{O}/\text{Fe}]$, and $[\text{Ce}/\text{Fe}]$ abundances for two stars in the innermost regions of NGC 6380, and by adopting the spectroscopic atmospheric parameters listed in Table 1. Each panel shows the best-fit synthesis (blue) from BACCHUS compared to the observed spectra (black squares) of selected lines (marked with black arrows, and cyan shadow bands of $3.2 \times 10^{-4} \mu\text{m}$ wide).

from high-quality APOGEE data taken from Mészáros et al. (2020).

We find a mean metallicity $\langle [\text{Fe}/\text{H}] \rangle$ between -0.80 and -0.73 for NGC 6380 depending on the adopted atmospheric parameters; within the uncertainties we do not detect any real spread in this element. Table 1 indicates that $[\text{Fe}/\text{H}]$ is systematically shifted within the internal uncertainties due to the adoption of a different T_{eff} and $\log g$ scales. However, given the small sample size of this work, the presence of an iron spread cannot be definitively ruled out, and will be investigated in future CAPOS papers (Geisler et al. 2021).

Overall, the chemical enrichment of NGC 6380 is in agreement with 47 Tucanae, whose metallicity is very similar to that of NGC 6380, within the observational errors, for almost all species except $[\text{Ce}/\text{Fe}]$ (see Figure 2), which displays enhancements above solar in NGC 6380, but below solar in

47 Tucanae. In addition, NGC 6380 exhibits a slightly larger spread ($\gtrsim 0.27$ dex) in $[\text{Ce}/\text{Fe}]$ that exceeds the typical observational uncertainties, while that of 47 Tucanae is smaller, as can be appreciated from inspection of Figures 4(c) and (f) and the results listed in Table 1.

Unfortunately, Mészáros et al. (2020) do not provide determinations for $[\text{Ti}/\text{Fe}]$ and $[\text{Ni}/\text{Fe}]$ for 47 Tucanae; however, our determinations (see mean values in Table 1) reveal that both chemical species in NGC 6380 are at the same typical levels as other MW GCs or field stars with similar metallicity (see, e.g., Villanova et al. 2019). This is also supported by the super-solar abundances of other α -elements (O, Mg, Si, and Ca), with a small star-to-star spread (not significantly larger than the typical error bars), being compatible with other GCs at similar metallicity such as 47 Tucanae (Figure 3). We conclude that the typical $[\text{Ti}/\text{Fe}]$ and $[\text{Si}/\text{Fe}]$ enrichment observed in NGC 6380, accompanied by its bulge-like orbit (Massari et al. 2019), suggests it may have formed in situ.

The odd-Z elements (Al, K) are also slightly overabundant compared to the Sun, with 1σ spreads between 0.08 and 0.11 dex in K, and ~ 0.17 dex in Al. Neither the Mg–K and Mg–Al anticorrelation nor the Si–Al and N–Al correlation are evident in NGC 6380. However, we notice that the mean $\langle [\text{Mg}/\text{Fe}] \rangle$ is between $+0.15$ and $+0.30$ (depending on the adopted atmospheric parameters), and is less abundant than that observed in 47 Tucanae at similar metallicity (see Figures 3 and 4), which could be related somehow with the large spread in Al observed in NGC 6380. However, it is important to note that, if the GC polluters are asymptotic giant branch (AGB) stars, then the observed large spread in Al seems to be at odds with the predicted yields of massive AGB stars, as models suggest a modest Mg–Al cycle with no Al enrichment above $[\text{Fe}/\text{H}] > -1.0$ (see e.g., Ventura et al. 2016; Mészáros et al. 2020).

Regarding the light elements (C, N), we find a very large variation ($\gtrsim 1.5$ dex) in N, which is clearly anticorrelated with C, and comparable to the extended variations in N and C observed in 47 Tucanae (see Figure 4(b)), giving support to the idea that NGC 6380 indeed has multiple populations based on N. Indeed, at the metallicity of NGC 6380, it is likely that only second-generation stars attain such high nitrogen abundances (see, e.g., Schiavon et al. 2017; Mészáros et al. 2020). Therefore, we conclude that NGC 6380 hosts MPs.

Figure 4(c) also shows that Ce is likely correlated with Al, albeit with a weaker amplitude, while Figure 4(f) exhibits an apparent correlation with the N abundance. The Pearson and Spearman correlation test between Ce and N is larger, with a p -value near zero, as indicated in the internal legend in Figures 4(c) and (f), indicating that the observed correlation is not due to random chance. It is important to note that the adoption of a different T_{eff} and $\log g$ scale produces a slightly less pronounced—but still present—correlation (as can be appreciated in Figures 4(c) and (f)), indicating an apparent correlation between Ce and the light elements. Additionally, as can be appreciated in Table 1, the observed star-to-star scatter in $[\text{Ce}/\text{Fe}]$ is larger ($\gtrsim 0.27$ dex) than the typical uncertainties in $[\text{Ce}/\text{Fe}]$ in individual stars. However, it is also important to note that the apparent correlation between Ce, N, and Al could be affected by (systematic and random) uncertainties, due, for instance, to the differential-reddening correlation and the adopted isochrones. Therefore, it is highly desirable to obtain additional observations to confirm this finding.

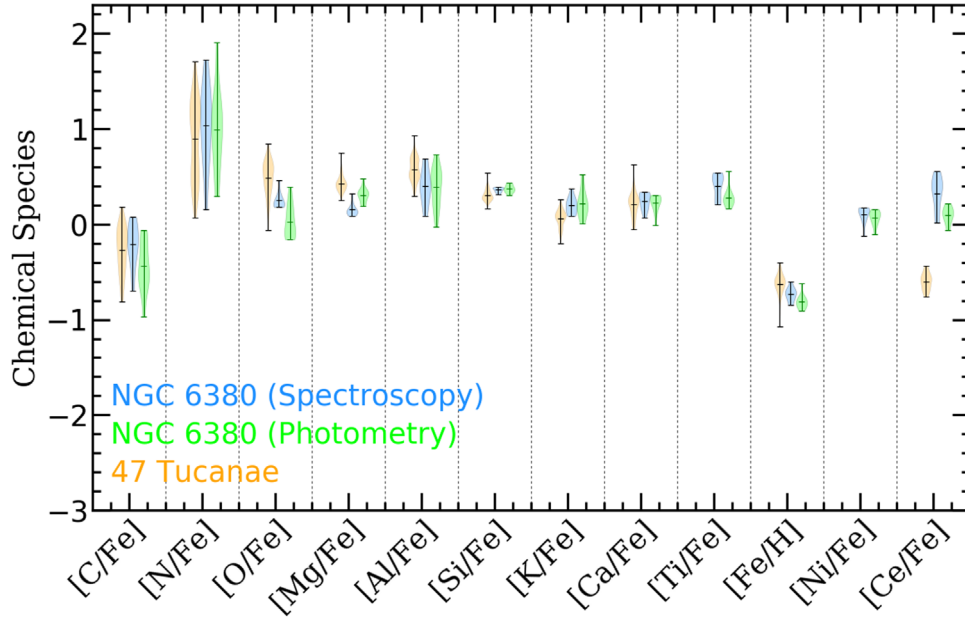


Figure 3. Elemental-abundance density estimation (violin representation) of NGC 6380 (dodgerblue), compared to elemental abundances of 47 Tucanae (orange) from Mészáros et al. (2020). Each violin representation indicates with lines the mean and limits of the distribution.

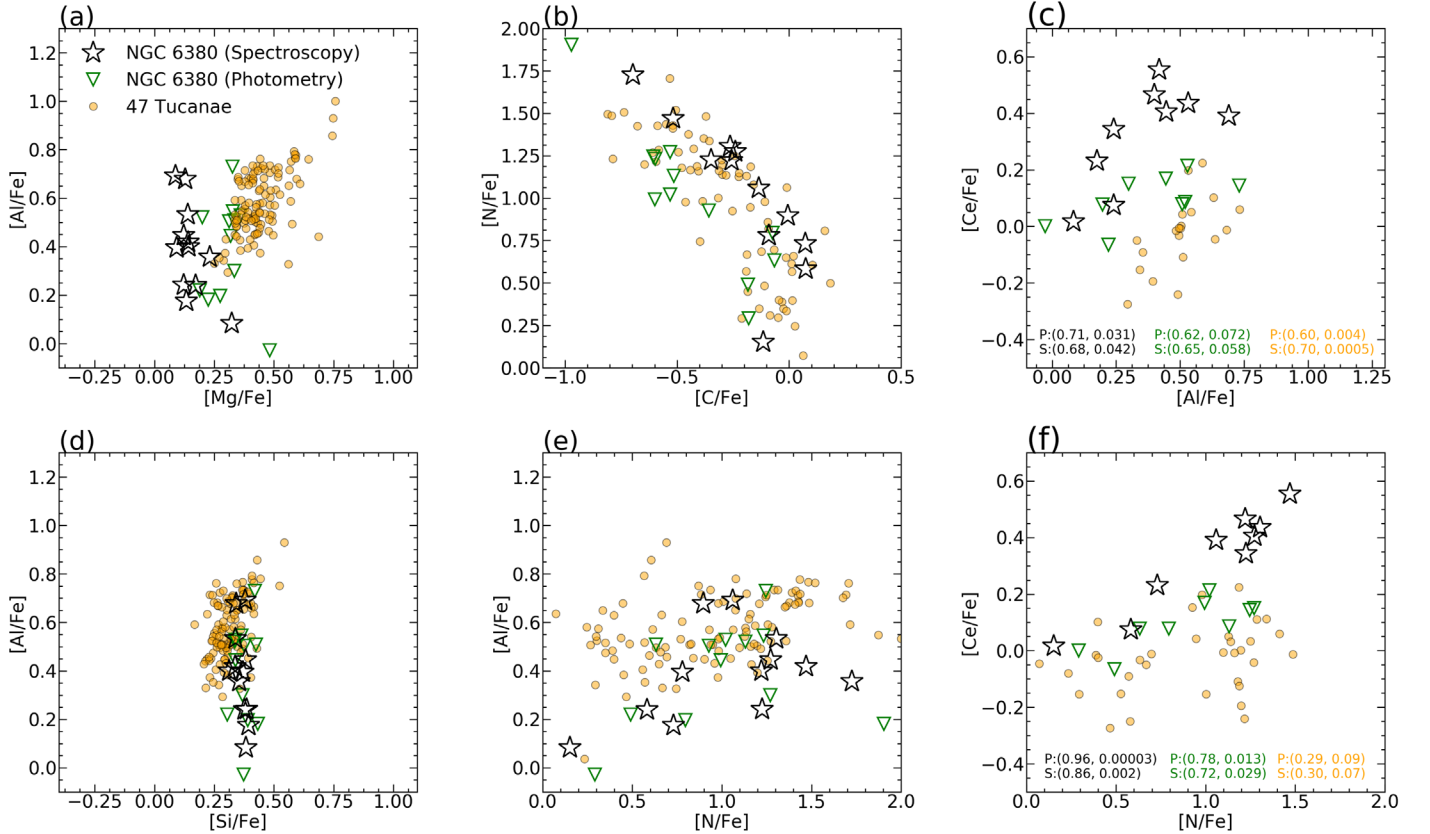


Figure 4. Panels (a)–(f): [Mg/Fe]–[Al/Fe], [C/Fe]–[N/Fe], [Al/Fe]–[Ce/Fe], [Si/Fe]–[Al/Fe], [N/Fe]–[Al/Fe], and [N/Fe]–[Ce/Fe] distributions for NGC 6380 (black stars) and 47 Tucanae (orange dots) stars. In panels (c) and (f), Pearson’s (P: first row of the annotation) and Spearman’s (S: second row of the annotation) coefficients (first entry) and p -values (second entry) are indicated for our determinations by adopting atmospheric parameters from spectroscopy (black annotation), photometry (green annotation), and 47 Tucanae (orange annotation). The typical uncertainties are listed in Table 1.

In addition to the N–Ce and Al–Ce correlations seen in NGC 6380 found in this work, we examined the APOGEE-2 GC data compiled by Mészáros et al. (2020), and found no significant correlation with Ce for other GCs at the APOGEE-2 database at a similar metallicity as NGC 6380, with the

exception of 47 Tucanae, which exhibits a marginal correlation of Al and N with Ce, as shown in Figures 4(c) and (f). It is important to note that NGC 6380 ($3.34 \times 10^5 M_{\odot}$) is less massive than 47 Tucanae ($8.95 \times 10^5 M_{\odot}$) according to the recent estimation by Baumgardt & Hilker (2018), likely

indicating a GCs mass threshold for the occurrence of N–Ce or Al–Ce correlations.

NGC 6380 is *the first case of a bulge GC where a N–Ce correlation has been detected*, likely indicating a different chemical evolution of this cluster with respect to the bulk of the MW GCs. Currently, a consensus interpretation of the origin for such N–Ce or Al–Ce correlations is still lacking.

The origins of the cerium abundance ratios and enhanced nitrogen are possibly related to AGB stars, as recently reconfirmed by Kobayashi et al. (2020). Cerium is produced primarily via the *s*-process in thermally pulsing (TP) AGB stars, while large amounts of primary nitrogen can be synthesized as a result of hot bottom burning in intermediate-mass AGB stars, where primary ^{12}C from triple- α burning is converted to ^{14}N in the deep convective envelope (e.g., Karakas & Lattanzio 2014). This could be an important indication that, in this cluster, the second-generation stars could be the product of yields from low- or intermediate-mass AGB stars (Ventura et al. 2009). The relatively high metallicity of NGC 6380 and the apparent increase of the Ce abundance as N increases could support this assertion. Another possible alternative could be fast-rotating massive stars (“spinstars”), which can also produce these secondary elements as primaries, due to the rotational mixing. These effects are mainly studied in metal-poor stars, but they were extended to different metallicities in Frischknecht et al. (2016) and Limongi & Chieffi (2018).

In conclusion, it is not presently possible to determine the origin of the N and Al correlations with the *s*-process element Ce, but clearly the data shows that they are correlated, since that is the expectation for production in these two possible sites (AGBs and spinstars). Further discussion regarding pollution scenarios require detailed computations and analysis, beyond the scope of the present work.

5. Conclusions

APOGEE-2S has enabled the first detailed study of the NGC 6380 cluster, which was not possible before given the high obscuration; therefore, no other determinations have ever been done from spectroscopy. Here, we report on the apparent discovery of a bulge GC (NGC 6380), at relatively high metallicity, $[\text{Fe}/\text{H}] \sim -0.80$ to -0.73 (depending on the adopted atmospheric parameters), where Ce is likely correlated with the N and Al abundances. By adopting different scales in the atmospheric parameters, we find systematic changes in some of the determined abundances ratios, yet the correlation between Ce with N and Al appear to remain.

The present analysis suggests two main results. (1) Slow neutron-capture element variation is likely present in the bulge GC NGC 6380. It is therefore worthwhile to explore if this variation exists in other GCs, particularly in the relatively high-metallicity regime. (2) Among the MPs in this GC, the Ce abundances appear to be correlated with those of N and Al, thus Ce could also be a multiple-population element. Different processes could be responsible for the puzzling N–Ce and Al–Ce correlations, likely indicating a different chemical-evolution history for bulge GCs at metallicities similar to NGC 6380 with respect to the bulk of MW GCs.


T.C.B. acknowledges partial support for this work from grant PHY 14-30152: Physics Frontier Center/JINA Center for the Evolution of the Elements (JINA-CEE), awarded by the US National Science Foundation. B.B. acknowledges grants from

FAPESP, CNPq, and CAPES—Financial code 001. D.G. acknowledges financial support from the Dirección de Investigación y Desarrollo de la Universidad de La Serena through the Programa de Incentivo a la Investigación de Académicos (PIA-DIDULS). D.G. and D.M. gratefully acknowledge support from the Chilean Centro de Excelencia en Astrofísica y Tecnologías Afines (CATA) BASAL grant AFB-170002.

Funding for the Sloan Digital Sky Survey IV has been provided by the Alfred P. Sloan Foundation, the U.S. Department of Energy Office of Science, and the Participating Institutions. SDSS-IV acknowledges support and resources from the Center for High-Performance Computing at the University of Utah. The SDSS website is www.sdss.org.

This work has made use of data from the European Space Agency (ESA) mission Gaia (<http://www.cosmos.esa.int/gaia>), processed by the Gaia Data Processing and Analysis Consortium (DPAC, <http://www.cosmos.esa.int/web/gaia/dpac/consortium>). Funding for the DPAC has been provided by national institutions, in particular the institutions participating in the Gaia Multilateral Agreement.

ORCID iDs

José G. Fernández-Trincado  <https://orcid.org/0000-0003-3526-5052>
 Timothy C. Beers  <https://orcid.org/0000-0003-4573-6233>
 Beatriz Barbuy  <https://orcid.org/0000-0001-9264-4417>
 Dante Minniti  <https://orcid.org/0000-0002-7064-099X>
 Sandro Villanova  <https://orcid.org/0000-0001-6205-1493>
 Doug Geisler  <https://orcid.org/0000-0002-3900-8208>
 Baitian Tang  <https://orcid.org/0000-0002-0066-0346>

References

- Ahumada, R., Prieto, C. A., Almeida, A., et al. 2020, *ApJS*, 249, 3
 Asplund, M., Grevesse, N., & Sauval, A. J. 2005, in *ASP Conf. Ser.* 336, *Cosmic Abundances as Records of Stellar Evolution and Nucleosynthesis*, ed. I. Barnes, G. Thomas, & F. N. Bash (San Francisco, CA: ASP), 25
 Bastian, N., & Lardo, C. 2018, *ARA&A*, 56, 83
 Baumgardt, H., & Hilker, M. 2018, *MNRAS*, 478, 1520
 Blanton, M. R., Bershady, M. A., Abolfathi, B., et al. 2017, *AJ*, 154, 28
 Bowen, I. S., & Vaughan, A. H. J. 1973, *ApOpt*, 12, 1430
 Bressan, A., Marigo, P., Girardi, L., et al. 2012, *MNRAS*, 427, 127
 Carretta, E., & Bragaglia, A. 2021, *A&A*, 646, A9
 Carretta, E., Bragaglia, A., Gratton, R., & Lucatello, S. 2009, *A&A*, 505, 139
 Carretta, E., Gratton, R. G., Bragaglia, A., et al. 2013, *ApJ*, 769, 40
 Cohen, J. G., & Kirby, E. N. 2012, *ApJ*, 760, 86
 Cohen, R. E., Bellini, A., Libralato, M., et al. 2021, *AJ*, 161, 41
 Djorgovski, S., & Meylan, G. 1993, in *ASP Conf. Ser.* 50, *Structure and Dynamics of Globular Cluster*, ed. S. G. Djorgovski & G. Meylan (San Francisco, CA: ASP), 325
 Fernández-Trincado, J. G., Beers, T. C., Minniti, D., et al. 2021a, *A&A*, 647, A64
 Fernández-Trincado, J. G., Beers, T. C., Minniti, D., et al. 2021b, *A&A*, 648, A70
 Fernández-Trincado, J. G., Minniti, D., Beers, T. C., et al. 2020, *A&A*, 643, A145
 Fernández-Trincado, J. G., Minniti, D., Souza, S. O., et al. 2021c, *ApJL*, 908, L42
 Fernández-Trincado, J. G., Zamora, O., Souto, D., et al. 2019, *A&A*, 627, A178
 Frischknecht, U., Hirschi, R., Pignatari, M., et al. 2016, *MNRAS*, 456, 1803
 García Pérez, A. E., Allende Prieto, C., Holtzman, J. A., et al. 2016, *AJ*, 151, 144
 Geisler, D., Villanova, S., O’Connell, J. E., et al. 2021, *A&A*, in press
 Gunn, J. E., Siegmund, W. A., Mannery, E. J., et al. 2006, *AJ*, 131, 2332
 Gustafsson, B., Edvardsson, B., Eriksson, K., et al. 2008, *A&A*, 486, 951
 Horta, D., Schiavon, R. P., Mackereth, J. T., et al. 2020, *MNRAS*, 493, 3363
 Karakas, A. I., & Lattanzio, J. C. 2014, *PASA*, 31, e030
 Kobayashi, C., Karakas, A. I., & Lugaro, M. 2020, *ApJ*, 900, 179

- Limongi, M., & Chieffi, A. 2018, *ApJS*, **237**, 13
- Majewski, S. R., Schiavon, R. P., Frinchaboy, P. M., et al. 2017, *AJ*, **154**, 94
- Marino, A. F., Milone, A. P., Renzini, A., et al. 2021, arXiv:2106.15978
- Massari, D., Koppelman, H. H., & Helmi, A. 2019, *A&A*, **630**, L4
- Masseron, T., García-Hernández, D. A., Mészáros, S., et al. 2019, *A&A*, **622**, A191
- Masseron, T., Merle, T., & Hawkins, K. 2016, BACCHUS: Brussels Automatic Code for Characterizing High accuracy Spectra, Astrophysics Source Code Library, ascl:1605.004
- Mészáros, S., Martell, S. L., Shetrone, M., et al. 2015, *AJ*, **149**, 153
- Mészáros, S., Masseron, T., García-Hernández, D. A., et al. 2020, *MNRAS*, **492**, 1641
- Mucciarelli, A., Bellazzini, M., Merle, T., et al. 2015, *ApJ*, **801**, 68
- Nataf, D. M., Wyse, R. F. G., Schiavon, R. P., et al. 2019, *AJ*, **158**, 14
- Nidever, D. L., Holtzman, J. A., Allende Prieto, C., et al. 2015, *AJ*, **150**, 173
- Ortolani, S., Bica, E., & Barbuy, B. 1998, *A&AS*, **127**, 471
- Pancino, E., Romano, D., Tang, B., et al. 2017, *A&A*, **601**, A112
- Pišmiš, P. 1959, *BOTT*, **2**, 37
- Renzini, A., D'Antona, F., Cassisi, S., et al. 2015, *MNRAS*, **454**, 4197
- Romero-Colmenares, M., Fernández-Trincado, J. G., Geisler, D., et al. 2021, *A&A*, in press
- Schiavon, R. P., Johnson, J. A., Frinchaboy, P. M., et al. 2017, *MNRAS*, **466**, 1010
- Smith, V. V., Bizyaev, D., Cunha, K., et al. 2021, *AJ*, **161**, 254
- Vasiliev, E., & Baumgardt, H. 2021, *MNRAS*, **505**, 5978
- Ventura, P., Caloi, V., D'Antona, F., et al. 2009, *MNRAS*, **399**, 934
- Ventura, P., García-Hernández, D. A., Dell'Agli, F., et al. 2016, *ApJL*, **831**, L17
- Villanova, S., Monaco, L., Geisler, D., et al. 2019, *ApJ*, **882**, 174
- Wilson, J. C., Hearty, F. R., Skrutskie, M. F., et al. 2019, *PASP*, **131**, 055001
- Zamora, O., García-Hernández, D. A., Allende Prieto, C., et al. 2015, *AJ*, **149**, 181
- Zasowski, G., Cohen, R. E., Chojnowski, S. D., et al. 2017, *AJ*, **154**, 198